Received December 2004
Revised July 2005
Accepted September 2005

Numerical analysis of natural convection in parallel, convergent, and divergent open-ended channels

Francisco Marcondes
Mechanical Engineering Department, Federal University of Ceará, Fortaleza, Brazil, and
Vinícius de Souza Melo and Jose Maurício Gurgel
Mechanical Technology Department, Federal University of Paraíba, João Pessoa, Brazil

Abstract

Purpose – To investigate the natural convection in open-ended parallel, convergent, and divergent channels using a fully elliptic procedure without extending the domain outside the channel for the application of the boundary conditions at the inlet and outlet of the channels.

Design/methodology/approach – The model is two-dimensional and fully elliptic in x and y directions, and the equations are solved only inside the channel by the finite volume method using a co-located arrangement with a segregated procedure and boundary fitted coordinates. The pressure-velocity coupling is solved by the PRIME algorithm.

Findings – The results are shown in terms of velocity vectors, streamlines, isotherms, and the local and the average Nusselt number for all fluids and configurations investigated. For high values of the Rayleigh number, a recirculation region in the outlet of all investigated configurations and Prandtl numbers was observed. Based on the results, a single correlation is proposed to evaluate the average Nusselt number for all fluids and configurations analyzed.

Research limitations/implications – The shown results are based on the following hypothesis: steady-state, two-dimensional, laminar flow, and Boussinesq's aproximation. The results are presented in following range of parameters: $10^5 < (S_{max}/L)Ra_{S_{max}} < 10^8$, where S_{max} denotes the maximum distance between the plates and Ra denotes the Rayleigh number; half angle of convergence or divergence (θ): 5° and 15°; and Prandtl numbers: 0.7, 5.0, and 88.

Originality/value – Local and average Nusselt numbers, for Prandtl numbers varying from 0.70 to 88, and a correlation for the average Nusselt number for all fluids and configurations are presented. The results presented in this paper are useful to engineers and researchers involved in thermal design and numerical methods.

Keywords Convection, Channel flow, Finite-volume methods

Paper type Research paper

Nomenclature

A	= Coefficients in the momentum, energy and pressure equations	F	= Correlation factor,
		g	= Gravity acceleration (m/s^2)
B	= Source term in the momentum, energy and pressure equations	H	= Height of the channel (m)
		J	= Jacobian of the transformation
C_1, C_2, C_4	= Transformed diffusion coefficients	L	= Channel length (m)

International Journal of Numerical Methods for Heat & Fluid Flow
Vol. 16 No. 3, 2006
pp. 304-323

0961-5539
DOI 10.1108/09615530610649735

k = Thermal conductivity (W/m K)
q''_y = Local heat flux (W/m^2 K)
Nu_l = Local Nusselt number
Nu_a = Average Nusselt number
P = Pressure (Pa)
Pe = Peclet number
Pr = Prandtl number
$\hat{P}^{\phi}$ = Transformed pressure source term
r = Residue vector
Ra = Rayleigh number
S = Channel width
$\hat{S}^{\phi}$ = Transformed source term in the equation for ϕ
t = Time (s)
T = Temperature (K)
u, v = Cartesian components of the velocity vector (m/s)
$\hat{u}, \hat{v}$ = Auxiliary Cartesian components of velocity components (m/s)
U, V = Contravariant components of the velocity vector (m^2/s)
$\hat{U}, \hat{V}$ = Auxiliary contravariant components of the velocity vector (m^2/s)
x, y = Coordinates in the Cartesian system
α, β, γ = Components of the metric tensor
$\bar{\alpha}, \bar{\beta}$ = Coefficients in the WUDS scheme
$\bar{\bar{\alpha}}$ = Thermal diffusivity (m^2/s)
$\bar{\bar{\beta}}$ = Thermal expansion coefficient (1/K)
ε = User-specified parameter
Γ = General diffusion coefficient
$\bar{\nu}$ = Kinematic viscosity (m^2/s)
ρ = Density (kg/m^3)
θ = Half convergent or divergent angle
ϕ = Scalar field
ξ, η = Coordinates in a general curvilinear system
|||| = Denotes euclidian norm

Subscripts

a = denotes average value
e, w, n, s = denotes control-volume interfaces
i = denotes values at channel entrance
l = denotes local value
m = denotes average value
max = denotes maximum value
min = denotes minimum value
o = denotes outside of the channel
$P, E, W, N, S, NE, SE, NW, SW$ = denotes control volumes
w = denotes parameters evaluated at the heated wall
ξ, η = partial derivates of first order

Superscripts

n = denotes quantities evaluated at the nth time level
o = denotes quantities evaluated at the old time level

Introduction

Natural convection in open-ended channels has been extensively studied due to its broad application spectrum in refrigeration, electronic equipment, grain drying, and solar collectors. This type of problem has been investigated through theoretical, numerical, and experimental procedures. However, most of the cases refer to natural convection between vertical and parallel plates. With respect to the numerical solutions, most of them neglect the diffusion terms in the streamwise direction, in the momentum and energy equations. In the present work, this type of methodology will be called the parabolic procedure. It should be noted that the parabolic procedure was largely used in the 1980s because of the restricted computational resources. Several authors employed this procedure for the solution of natural convection in vertical and

parallel channels (Bodoia and Osterle, 1962; Aung *et al.*, 1972; Aihara, 1973; Aung and Worku, 1986). Despite its large application, the parabolic procedure still has some difficulties to overcome. The first one is that velocity and pressure in the inlet channel are not known for a specified height of the channel (Maliska and Marcondes, 1993). Another difficulty and perhaps the most restrictive one is that the parabolic procedure cannot capture recirculating regions, for example, in the outlet of vertical channels with an isothermal wall and an isolated one (Sparrow *et al.*, 1984), and in the outlet of divergent channels with both walls at the same temperature (Sparrow *et al.*, 1988). In those cases, the diffusion terms in the streamwise direction need to be included in the conservation equations giving rise to a fully elliptic procedure.

The main issues to be addressed in a fully elliptic procedure are the unknown pressure and velocity in the inlet channel. Some works by-passed this difficulty by extending the domain outside the channel where the buoyancy forces are absent (Kettleborough, 1972; Nakamura *et al.*, 1982; Naylor *et al.*, 1991; Campo *et al.*, 1999; Morrone, 2001; Da Silva *et al.*, 2004). However, it should be noted that one problem with this procedure is the creation of additional unknowns outside the domain. Another route is to solve the conservation equation only in the channel, but this procedure requires that other equations be used to evaluate both pressure and velocity in the inlet channel. Nieckele and Azevedo (1987) studied the natural convection in parallel vertical channels with one wall at a prescribed temperature and the other one insulated. They presented numerical and experimental results, with the former obtained by the fully elliptic and parabolic procedures. Said (1996) presented results for the natural convection in convergent channels using a fully elliptic procedure. Marcondes and Maliska (1999) using an elliptic procedure solved the problem of natural convection in *L*-shaped channels. These equations were solved only in the channel. Additional equations were created to advance the pressure and velocity in the inlet channel, and the results were presented for air and water. Kaiser *et al.* (2004) investigated the natural convection in convergent channels by a fully implicit formulation using two codes: fluent and phoenics. They prescribed Bernoulli's equation at the channel inlet and the ambient pressure at the channel outlet.

Kihm *et al.* (1993) presented experimental results for air for converging channels using a specklegram technique. Shalash *et al.* (1997) presented experimental and numerical results for the convergent channel for air. They used a fully elliptic procedure and extended the domain at the channel inlet and outlet. Sparrow and Ruiz (1988) studied natural convection in vertical parallel, convergent, and divergent channels. They presented experimental and numerical results for water. The parabolic procedure was used to obtain the numerical results.

The goal of this paper is to analyze natural convection in vertical parallel, convergent, and divergent channels. Figure 1 shows the domains with its main geometrical characteristics. For each configuration, the influence of the Prandtl number and $(S_{\max}/L)Ra_{S_{\max}}$ parameter, where $Ra_{S_{\max}}$ is the Rayleigh number based on the maximum distance between plates, was studied. The fully elliptic procedure was employed, and the velocity and pressure in the inlet channel were adjusted as proposed by Marcondes and Maliska (1999). The conservation equations written in a generalized system of coordinates were solved by the finite volume method using a co-located arrangement. To treat the pressure-velocity coupling, the pressure implicit, momentum explicit (PRIME) algorithm was used. The results are presented using isotherms,

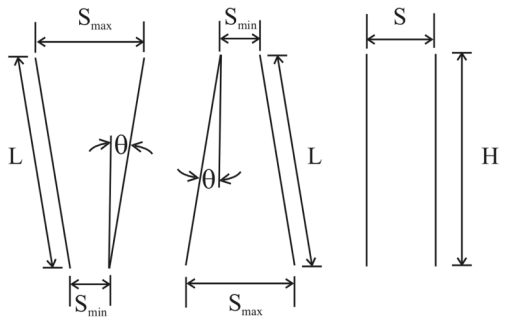

Figure 1.
Analyzed channels

streamlines, and the local and the average Nusselt number for Prandtl number varying from 0.7 to 88. A correlation capable of evaluating the average Nusselt number as a function of both Prandtl number and $(S_{\max}/L)Ra_{S_{\max}}$ parameter for all the Prandtl numbers and investigated configurations is also proposed.

Mathematical formulation

The present work deals with the numerical solution of two-dimensional natural convection in open-ended channels according to Figure 1. Assuming laminar and incompressible flow, Boussinesq approximation, and Newtonian fluid, the equations for mass conservation, momentum in the x and y directions, and energy can be written in a generalized curvilinear system (ξ, η) (Maliska 1995) as:

$$\frac{\partial}{\partial \xi}(\rho U) + \frac{\partial}{\partial \eta}(\rho V) = 0 \tag{1}$$

$$\frac{1}{J}\frac{\partial}{\partial t}(\rho u) + \frac{\partial}{\partial \xi}(\rho U u) + \frac{\partial}{\partial \eta}(\rho V u) = \frac{\partial}{\partial \xi}\left(C_1\frac{\partial u}{\partial \xi} + C_2\frac{\partial u}{\partial \eta}\right) + \frac{\partial}{\partial \eta}\left(C_2\frac{\partial u}{\partial \xi} + C_4\frac{\partial u}{\partial \eta}\right) + \hat{S}^u - \hat{P}^u \tag{2}$$

$$\frac{1}{J}\frac{\partial}{\partial t}(\rho v) + \frac{\partial}{\partial \xi}(\rho U v) + \frac{\partial}{\partial \eta}(\rho V v) = \frac{\partial}{\partial \xi}\left(C_1\frac{\partial v}{\partial \xi} + C_2\frac{\partial v}{\partial \eta}\right) + \frac{\partial}{\partial \eta}\left(C_2\frac{\partial v}{\partial \xi} + C_4\frac{\partial v}{\partial \eta}\right) + \hat{S}^v - \hat{P}^v \tag{3}$$

$$\frac{1}{J}\frac{\partial}{\partial t}(\rho T) + \frac{\partial}{\partial \xi}(\rho U T) + \frac{\partial}{\partial \eta}(\rho V T) = \frac{\partial}{\partial \xi}\left(C_1\frac{\partial T}{\partial \xi} + C_2\frac{\partial T}{\partial \eta}\right) + \frac{\partial}{\partial \eta}\left(C_2\frac{\partial T}{\partial \xi} + C_4\frac{\partial T}{\partial \eta}\right) + \hat{S}^T \tag{4}$$

where

$$
\begin{aligned}
P^u &= \frac{\partial P}{\partial \xi} y_\eta - \frac{\partial P}{\partial \eta} y_\xi & P^v &= \tfrac{\partial P}{\partial \eta} x_\xi - \tfrac{\partial P}{\partial \xi} x_\eta \\
S^u &= S^T = 0 & S^v &= \rho g \bar{\bar{\beta}} (T - T_o) \\
C_1 &= \alpha J \Gamma^\phi & C_2 &= -\beta J \Gamma^\phi \\
C_4 &= \gamma J \Gamma^\phi & \beta &= x_\xi x_\eta + y_\xi y_\eta \\
\alpha &= x_\xi^2 + y_\xi^2 & U &= y_\eta u - x_\eta v \\
\gamma &= x_\eta^2 + y_\eta^2 & V &= x_\xi v - y_\xi u \\
\hat{P}^\phi &= \tfrac{P^\phi}{J} & \hat{S}^\phi &= \tfrac{S^\phi}{J}
\end{aligned} \tag{5}
$$

Equations (1)-(4) can be written for a scalar ϕ as:

$$
\frac{1}{J}\frac{\partial}{\partial t}(\rho\phi) + \frac{\partial}{\partial \xi}(\rho U \phi) + \frac{\partial}{\partial \eta}(\rho V \phi) = \frac{\partial}{\partial \xi}\left(C_1 \frac{\partial \phi}{\partial \xi} + C_2 \frac{\partial \phi}{\partial \eta}\right) + \frac{\partial}{\partial \eta}\left(C_2 \frac{\partial \phi}{\partial \xi} + C_4 \frac{\partial \phi}{\partial \eta}\right) - \hat{P}^\phi + \hat{S}^\phi \tag{6}
$$

When $\phi = 1$, the mass conservation is obtained and for ϕ equal to u, v, and T, the momentum, and energy equation are recovered, respectively. Since only steady-state solutions are of interest, the transient terms in the momentum and energy equations were retained just for the iteration procedure.

Numerical procedure

Figure 2(a) shows the control volume used to integrate equation (6) in space. Figure 2 also shows the co-located grid layout. To evaluate the properties and their gradients on the faces of each control volume, the weight upstream difference scheme (WUDS), Raithby and Torrance (1974), was used. Integrating equation (6) into the control volume of Figure 2(a) and time, and using a WUDS scheme, we obtain the following equation for ϕ:

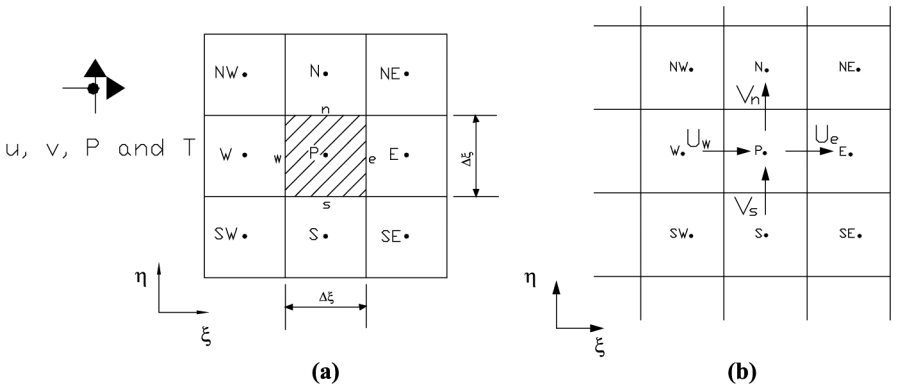

Figure 2.
(a) Elemental control volume and grid layout; (b) control volume for mass conservation

$$A_p\phi_P = A_e\phi_E + A_w\phi_W + A_n\phi_N + A_s\phi_S + A_{ne}\phi_{NE} + A_{nw}\phi_{NW} + A_{se}\phi_{SE} + A_{sw}\phi_{SW} - L[\hat{P}^{\phi}] + L[\hat{S}^{\phi}] \quad (7)$$

where, for example, A_e and A_p are given by:

$$A_e = -\dot{M}_e\left(\frac{1}{2} - \bar{\alpha}_e\right) + \frac{C_{1e}\bar{\beta}_e\Delta\eta}{\Delta\xi} - \frac{(C_{2n} - C_{2s})\Delta\eta}{4\Delta\xi} \quad (8)$$

$$A_p = \sum(A_{nb}) + \frac{M_p^o}{\Delta t} \quad (9)$$

Pressure equation

Integrating the mass conservation equation into the control volume of Figure 2(b), the following equation is obtained:

$$(U_e - U_w)\Delta\eta + (V_n - V_s)\Delta\xi = 0 \quad (10)$$

It can be observed from equation (10) that the contravariant velocities are necessary in the control volume faces. However, the Cartesian velocities that are used to evaluate those velocities are only known in the center of each control volume. If the values of the Cartesian velocities are available in the faces of the control volumes, the contravariant velocity in the east face, for example, is given by:

$$U_e = \hat{U}_e - \left[\alpha\frac{\partial P}{\partial\xi} + \beta\frac{\partial P}{\partial\eta}\right]_e d_e \quad (11)$$

Therefore, it is necessary to extrapolate the Cartesian velocities and the d coefficient from the center of the control volume to the interfaces. To calculate d on each control volume interface, the average of the neighborhood control volumes was adopted (Maliska, 1995). For the Cartesian velocities, a simple average can produce a poor coupling between pressure and velocity. Hence, the procedure suggested by Maliska (1995) and Santos *et al.* (1995) was used. Considering again the east face, the velocity $\hat{u}_e$ referred to Figure 3, is given by:

$$\hat{u}_e = \frac{\left[\begin{array}{c}\sum A_{nb}(u_{NB} - u_P)_P + \sum A_{nb}(u_{NB} - u_p)_E + \sum(A_{nb})_E u_e + \sum(A_{nb})_P u_e + B_u|_P \\ + B_u|_E + \rho^o\left.\frac{\Delta V}{\Delta t}\right|_P u_e + \rho^o\left.\frac{\Delta V}{\Delta t}\right|_E u_e\end{array}\right]}{\left[\rho^o\left.\frac{\Delta V}{\Delta t}\right|_P + \rho^o\left.\frac{\Delta V}{\Delta t}\right|_E + \sum(A_{nb})_E + \sum(A_{nb})_P\right]} \quad (12)$$

A similar expression was adopted to obtain $\hat{v}_e$. It should be emphasized that this procedure produces steady-state solutions that are independent of the chosen time-step. Doing the same procedure for the other faces of the control volume and replacing equation (12) and its counterparts for the other faces of the control volume, the following equation for pressure is obtained:

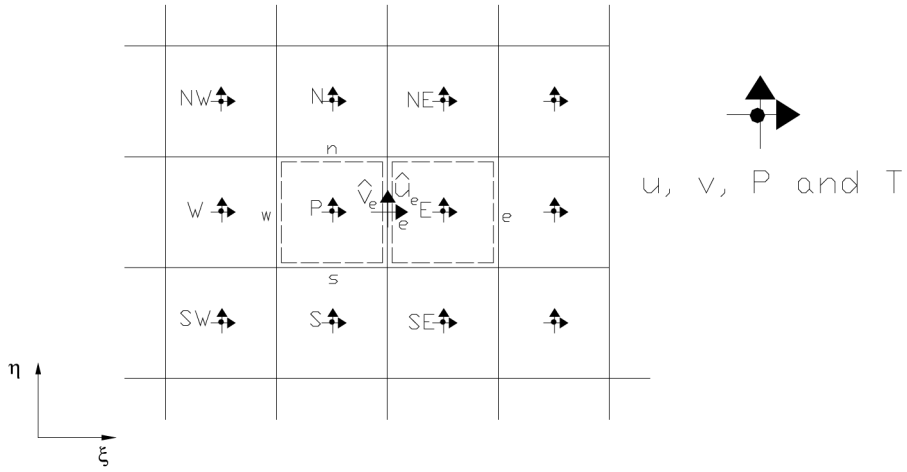

Figure 3.
Velocities involved in the $\hat{u}_e$ calculation

$$A_pP_P = A_eP_E + A_wP_W + A_nP_N + A_sP_S + A_{ne}P_{NE} + A_{nw}P_{NW} + A_{se}P_{SE} + A_{sw}P_{SW} + \nabla \cdot \vec{\hat{V}} \tag{13}$$

Solution procedure

The iterative process to obtain a converged solution is described in the following steps:

- estimate the initial u, v, and T fields;
- calculate the coefficients and sources terms for the momentum equations;
- solve the pressure equation, equation (13);
- compute U and V in the control volume faces, so that they satisfy mass conservation;
- compute U and V in the center of each control volume;
- compute u and v in the center of each control volume;
- solve the linear system for the energy equation; and
- if necessary return to step 2 to handle nonlinearities and interequation coupling.

The linear systems of P and T equations were solved by the generalized minimum residual (GMRES) algorithm, Saad and Schultz (1986) with an ILU (1) preconditioning. These linear systems were solved until $\|r\|/\|r_o\| < 10^{-4}$, in which $\|r\|$ denotes the Euclidean norm of the residue after a specified number of iterations and $\|r_o\|$ denotes the initial Euclidean norm of the residue. As a global convergence criteria, the following criteria in u and v (Maliska, 1995), was used:

$$\frac{\phi^{n+l} - \phi^n}{|\phi_{\max} - \phi_{\min}|} < \varepsilon \tag{14}$$

where $|\phi_{max} - \phi_{min}|$ stands for the maximum difference in u or v in the nth iteration. For most cases, ε equal to 10^{-5} was used. For the cases where some differences between the experimental and numerical results were observed, a tight criteria of 5×10^{-6} was used.

Boundary conditions

For the application of boundary conditions, a similar process to the inner control volumes was implemented. In the walls, a Dirichlet boundary condition was prescribed, and at the outlet channel parabolic conditions were used for all variables. At the inlet channel, the temperature was assumed to be equal to the external one. To evaluate the Cartesian velocity at the channel inlet, a similar process to that proposed by Marcondes and Maliska (1999) was used, and the pressure at the channel inlet was calculated by Bernoulli's equation:

$$P_i = -\frac{1}{2}\rho\left(u_i^2 + v_i^2\right) \tag{15}$$

Results and discussion

A mesh refinement study was realized for all investigated channels and fluids. For most cases, a relative variation less than 2 percent was obtained with 32×60 volumes; thus, this mesh was used for most of the cases presented in this section. For those cases where a variation larger than 2 percent was obtained, a mesh with 42×70 volumes was used. Table I presents the results of the mesh refinement for all the investigated configurations and fluids.

Now the results for the parallel, divergent, and convergent vertical channels for Prandtl number equal 5.0 will be presented. Figures 4 and 5 show the streamlines, isotherms, and velocity vectors for straight channels for $(S/H)Ra_S$ equal to 10^5 and 10^7, respectively. The Rayleigh number was defined by:

$$Ra_S = \frac{\rho g \bar{\bar{\beta}}(T_w - T_o)S^3}{\bar{\bar{\nu}}\bar{\bar{\alpha}}} \tag{16}$$

From Figures 4 and 5, it can be inferred that the fluid near the wall is accelerated. Therefore, the velocity in the core channel is lower than that near the wall. If the buoyancy effects increase, the velocity in the core region becomes negative as can be observed in Figure 5 to $(S/H)Ra_S = 10^7$. It can be also observed that due to the fact that Prandtl number is larger than 1, the hydrodynamic boundary layers are thicker than the thermal ones.

Mesh	$Nu_{a,S_{max}}$								
	Parallel			Convergent (5°)			Divergent (5°)		
	$Pr = 0.7$	$Pr = 5.0$	$Pr = 88$	$Pr = 0.7$	$Pr = 5.0$	$Pr = 88$	$Pr = 0.7$	$Pr = 5.0$	$Pr = 88$
22×50	28.96	33.34	34.99	32.42	37.66	40.26	33.38	39.53	42.72
32×60	32.42	38.21	40.45	32.10	37.23	40.02	33.68	39.49	42.35
42×70	33.01	38.72	41.86	31.39	36.42	39.24	34.98	39.42	40.99
52×80	32.60	37.886	41.10	30.90	35.82	38.66	34.55	38.63	40.01

Table I. Mesh study refinement for all configurations and Prandtl numbers

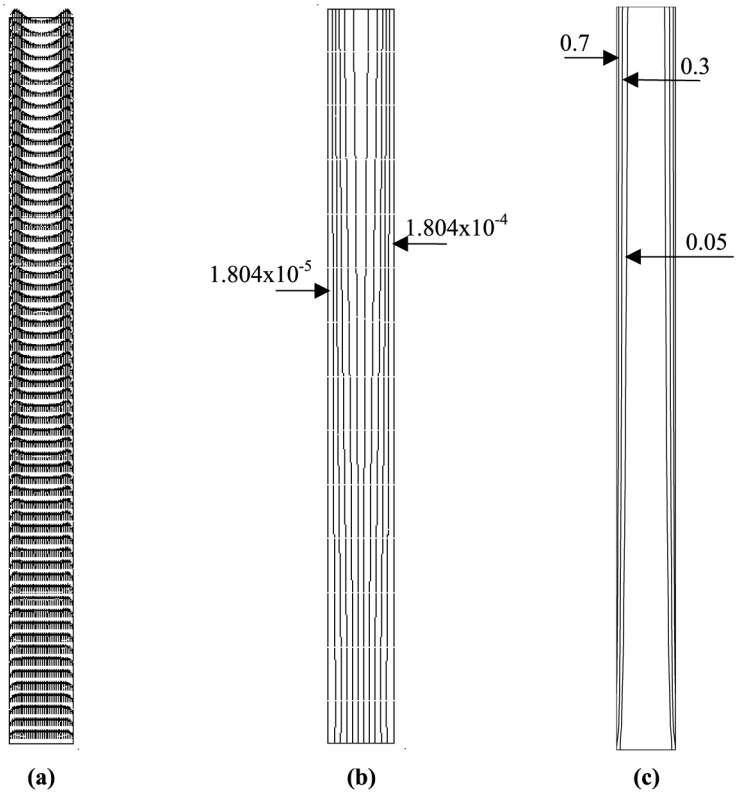

Figure 4.
Straight vertical channel for $Pr = 5.0$ and $(S/H)Ra_S = 10^5$ ($S = 0.01274$ m, $H = 0.1452$ m) (a) velocity vectors; (b) streamlines; (c) isotherms

Figure 6 shows the local Nusselt number for three $(S/H)Ra_S$ parameters. The local Nusselt number is given by:

$$Nu_{l,S} = \frac{q''_y S}{k(T_w - T_o)} \tag{17}$$

where $q''y$ is the heat flux in the y coordinate and k is the thermal conductivity of the fluid. From Figure 6, it can be observed that the local Nusselt number resembles the behavior of a thermal fully developed flow at small distances from the channel inlet, with this effect being more noticeable for small values of the $(S/H)Ra_S$ parameter.

The following results for convergent and divergent channels are based on the length of the plate (L) and in the maximum distance of the plates (S_{max}). The parameters (S,H) were changed since Sparrow and Ruiz (1988) observed that the results for parallel, convergent, and divergent channels can be fitted by only one correlation if those parameters were used.

Figures 7 and 8 show the velocity vectors, streamlines, and isotherms for the convergent channels for half angle of convergence of 5°, for two values of the

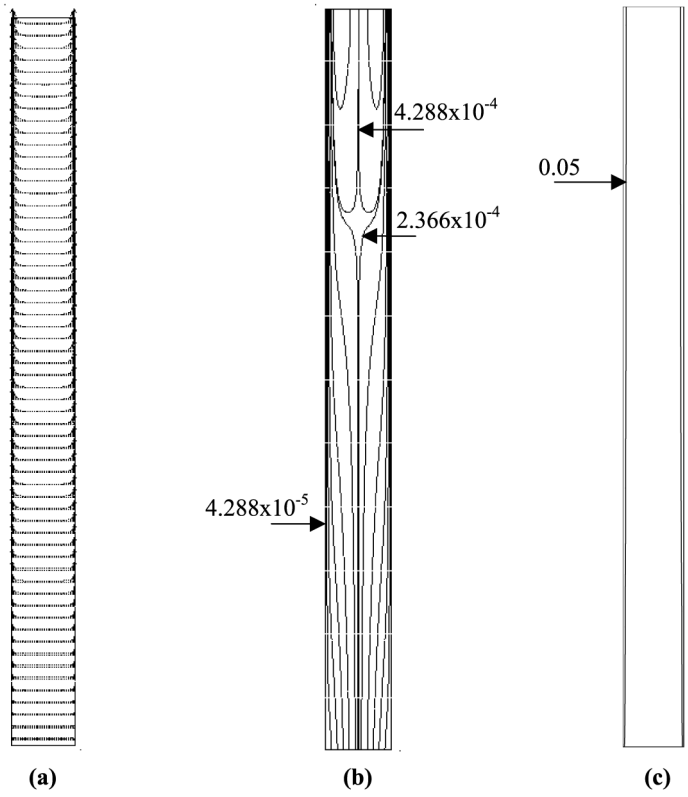

Figure 5.
Straight vertical channel for $Pr = 5.0$ and $(S/H)Ra_S = 10^7$ ($S = 0.01274$ m, $H = 0.1452$ m) (a) velocity vectors; (b) streamlines; (c) isotherms

$(S_{max}/L)Ra_{S_{max}}$ parameter. It can be noted from those figures that the boundary layers are thicker than those presented to the straight channel for the same value of the $(S_{max}/L)Ra_{S_{max}}$ parameter. Moreover, for high values of the $(S_{max}/L)Ra_{S_{max}}$ parameter, recirculating zones near the channel outlet were observed as can be seen in Figure 8. Those recirculation regions were not mentioned by Sparrow *et al.* (1988). However, it should be noted that the main flow is pushed toward the wall by buoyancy forces. Hence, it is necessary that external fluid be admitted through the exit to satisfy the mass conservation. Those recirculation regions were also observed in straight vertical channels, when buoyancy forces were increased. Finally, a tight stopping criteria was used, and the results were identical to those shown in Figures 7 and 8.

Figures 9 and 10 show the results obtained for 5° divergent channels. Sparrow and Ruiz (1988) observed a recirculating region near the outside of those channels. Although the heat transfer reaches a steady-state condition in a few minutes, a tendency to stabilize the recirculation region was not observed. In fact, it became deeper toward the channel inlet as time evolved. As described in the mathematical formulation, we are interested in the steady-state solutions. Therefore, it was not

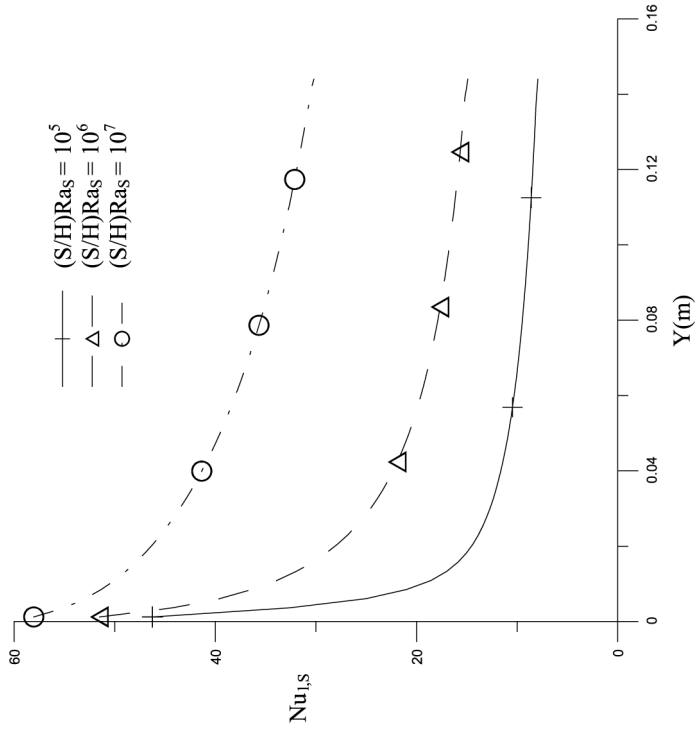

Figure 6.
Local Nusselt number for straight vertical channel for $Pr = 5.0$, $S = 0.01274$ m, and $H = 0.1452$ m

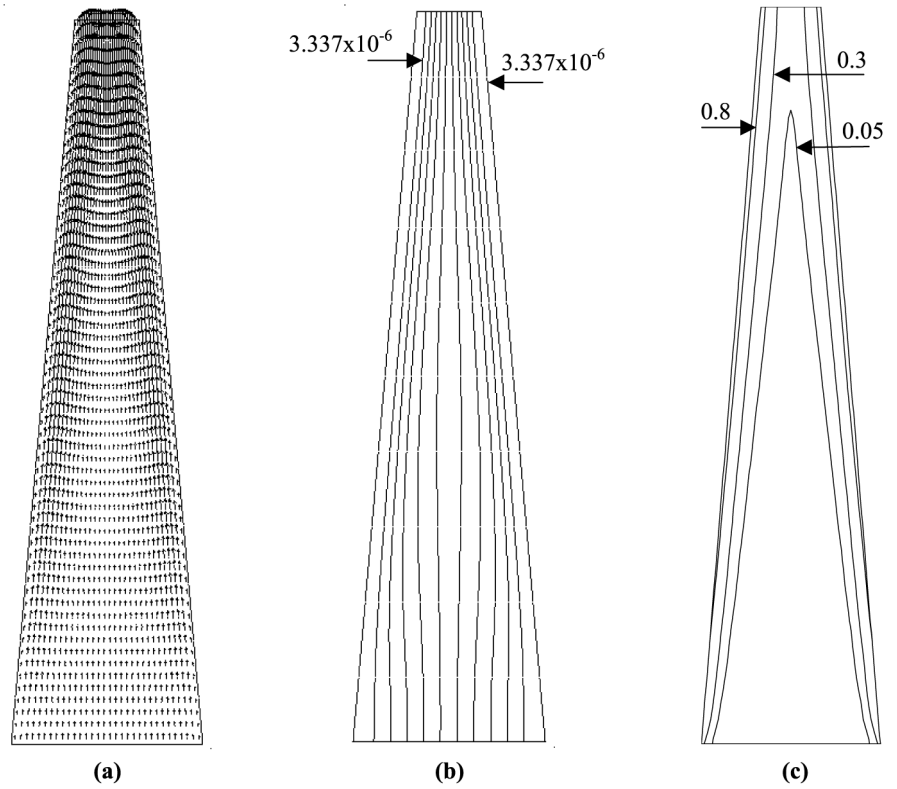

Figure 7.
Convergent vertical channel ($\theta = 5°$). $(S_{max}/L)Ra_{S_{max}} = 10^5$, $S_{max} = 0.03805$ m, $L = 0.1452$ m (a) velocity vectors; (b) streamlines; (c) isotherms

possible to notice this behavior. However, as the buoyancy effects were increased, the steady state recirculation region was observed in the outlet channel. From Figures 9 and 10, it can be noticed that the central region of the channel is almost stagnant while high velocity are observed near the walls. Thus, the temperature gradients are located very close to the walls. Even though the results for 15° divergent channels are not shown, those effects are more pronounced, and this effect increases the heat transfer in the channel. In fact, there exists a maximum angle that triggers the maximum heat transfer, but this effect was not studied in the present work. From the figures just presented, it is also possible to observe that the stagnant inner region increases with the $(S_{max}/L)Ra_{S_{max}}$ parameter.

Figure 11 shows the behavior of the local Nusselt number for both convergent (a) and divergent (b) channels. Comparing the results for parallel channels with the ones shown in Figure 11(a), a reduction in the local Nusselt number for convergent channels as compared to the former ones can be observed. As discussed by Incropera and DeWitt (1990), for natural convection in inclined plates, there is a reduction in buoyancy force along the plate. For convergent channels, the normal buoyancy force acts to maintain the ascending boundary layer flow in contact

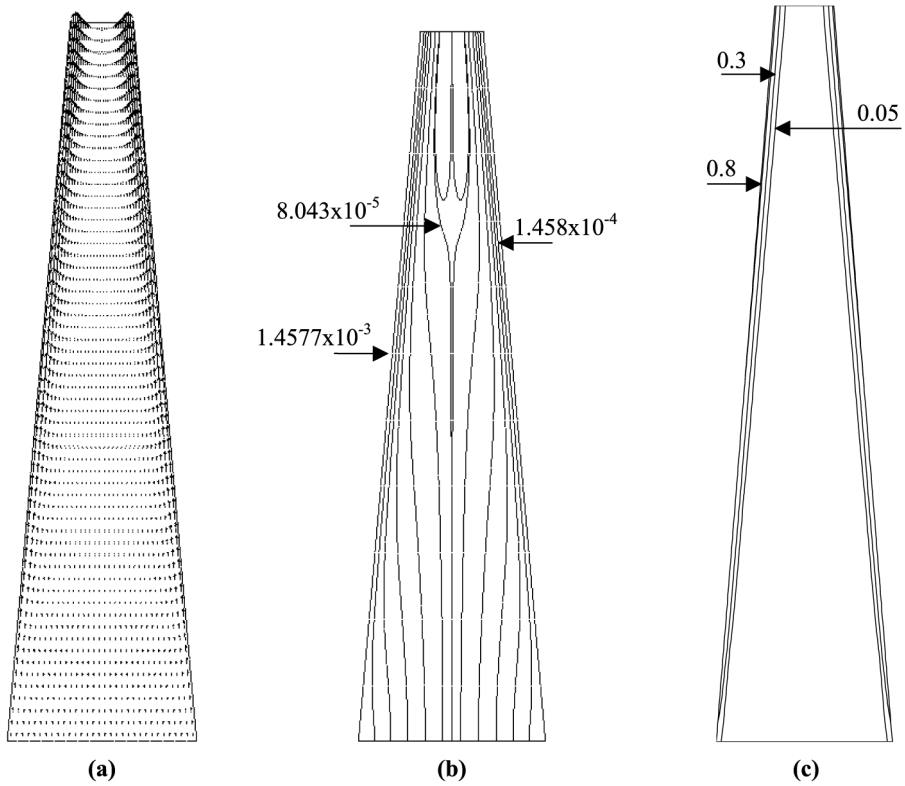

Figure 8.
Convergent vertical channel ($\theta = 5°$). $(S_{max}/L)Ra_{S_{max}} = 10^7$, $S_{max} = 0.03805$ m, $L = 0.1452$ m (a) velocity vectors; (b) streamlines; (c) isotherms

with the plate, thus reducing the velocity along the plate and, hence, the heat transfer when compared with parallel channel with the same $(S/H)Ras$ parameter. Another important issue that was observed in the convergent channel was the local increasing in the Nusselt number with this effect being intensified with the increase of the convergence angle. The increase of the local Nusselt number occurs due to the fluid acceleration and possible interaction of the recirculation zone with the thermal boundary layer. Comparing the results for divergent channels with those for convergent ones, for the same $(S_{max}/L)Ra_{S_{max}}$ parameter and angle, it is noticed that there exists a substantial increase in the local Nusselt number for the same position along the plate. Again, the plate position relatively to the fluid flow should be considered. For the convergent channel, the fluid flow must be deviated from the wall to flow along it. For divergent channels, the normal and parallel buoyancy forces act to push the fluid to the channel outlet. Therefore, an increase in the velocity along the walls is expected, and, in turn, in the local heat transfer. Those effects can be verified comparing the thermal and hydrodynamic boundary layers shown in Figures 7-10 for convergent and divergent channels. Finally, it can be seen that the optimal angle for divergent channel should be less than 5° since the results for 5 and 15° were almost similar.

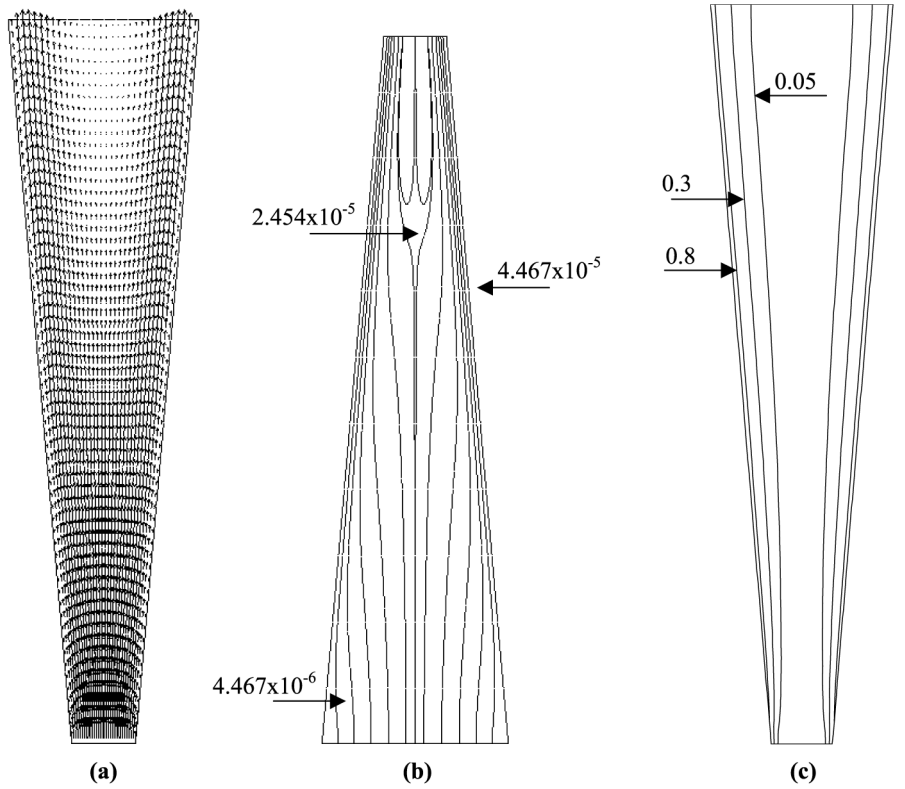

Figure 9.
Divergent vertical channel ($\theta = 5°$). $(S_{max}/L)Ra_{S_{max}} = 10^5$, $S_{max} = 0.03805$ m, $L = 0.1452$ m (a) velocity vectors; (b) streamlines; (c) isotherms

Now we present the average Nusselt number for Prandtl number ranging from 0.7 to 88, which cover fluids from air to oil, for all the analyzed configurations. Figure 12(a) shows the Nusselt number for Prandtl 5.0. The correlation proposed by Sparrow and Ruiz (1988) for parallel, convergent, and divergent channels and $Pr = 5.0$ is also shown in Figure 12(a). This correlation is given by:

$$Nu_{a,S_{max}} = 0.740\left(\left(\frac{S_{max}}{L}\right)Ra_{S_{max}}\right)^{0.24} \tag{18}$$

It can be seen from Figure 12(a) that a reasonable agreement between the calculations and the correlation proposed by Sparrow and Ruiz (1988) exists, but to some values at $(S_{max}/L)Ra_{S_{max}} = 10^8$. The maximum deviation was smaller than 19 percent and occurred for the divergent channel.

Figure 12(b) and (c) shows the average Nusselt number for Prandtl number 0.7 and 88. Comparing the data from Figure 12(b) and (c) with those in Figure 12(a), it can seen that the Nusselt numbers for $Pr = 5$ are very close to those for $Pr = 88$, while the Nusselt number for $Pr = 0.7$ are approximately 20 percent lower than those for $Pr = 5.0$, especially for small values of $(S_{max}/L)Ra_{S_{max}}$.

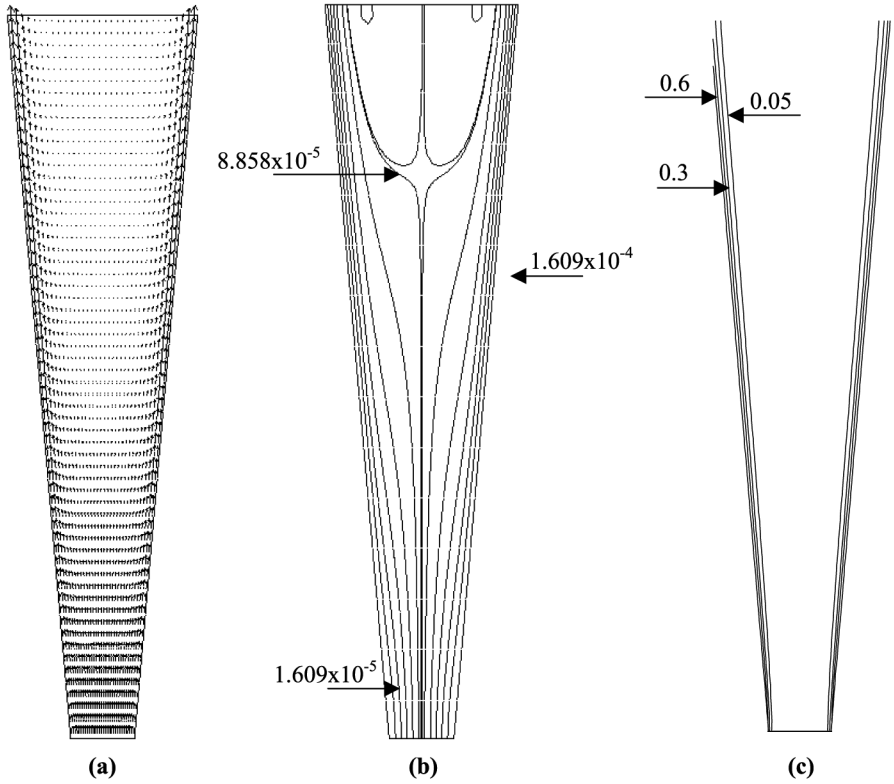

Figure 10.
Divergent vertical channel ($\theta = 5°$). $(S_{max}/L)Ra_{S_{max}} = 10^7$, $S_{max} = 0.03805$ m, $L = 0.1452$ m (a) velocity vectors; (b) streamlines; (c) isotherms

Finally, in order to put all the average Nusselt number data together, a correction factor, $F = 1/(1 + 1/Pr)$, is included in equation (18). The reason for this correction factor can be justified by scale analysis Bejan (1995), which shows $N\tilde{u}(Ra\,Pr)^n$ for low Prandtl number, and $N\tilde{u}(Ra)^n$ for high Prandtl numbers, where n is a constant and $\sim$ means the same order of magnitude. This procedure was successfully employed by Peter *et al.* (1993) in obtaining the results for one-sided heated vertical channel with the Prandtl number varying from 0.7 to 40. After incorporating the correction factor into equation (18) and adjusting the coefficient to obtain the same Nu values of equation (18) for $Pr = 5$, we obtain the following equation:

$$Nu_{a,S_{max}} = 0.773\left(\left(\frac{S_{max}}{L}\right)Ra_{S_{max}}F\right)^{0.24} \tag{19}$$

The average Nusselt number for all configurations and Prandtl numbers analyzed versus equation (19) are shown in Figure 13. It can be observed that a discrepancy between the obtained values and those proposed by the correlation exists. However, this discrepancy was smaller than 19 percent. It should be noted that the greatest discrepancy occurred for divergent channels (5 and 15°) and Prandtl number 0.7.

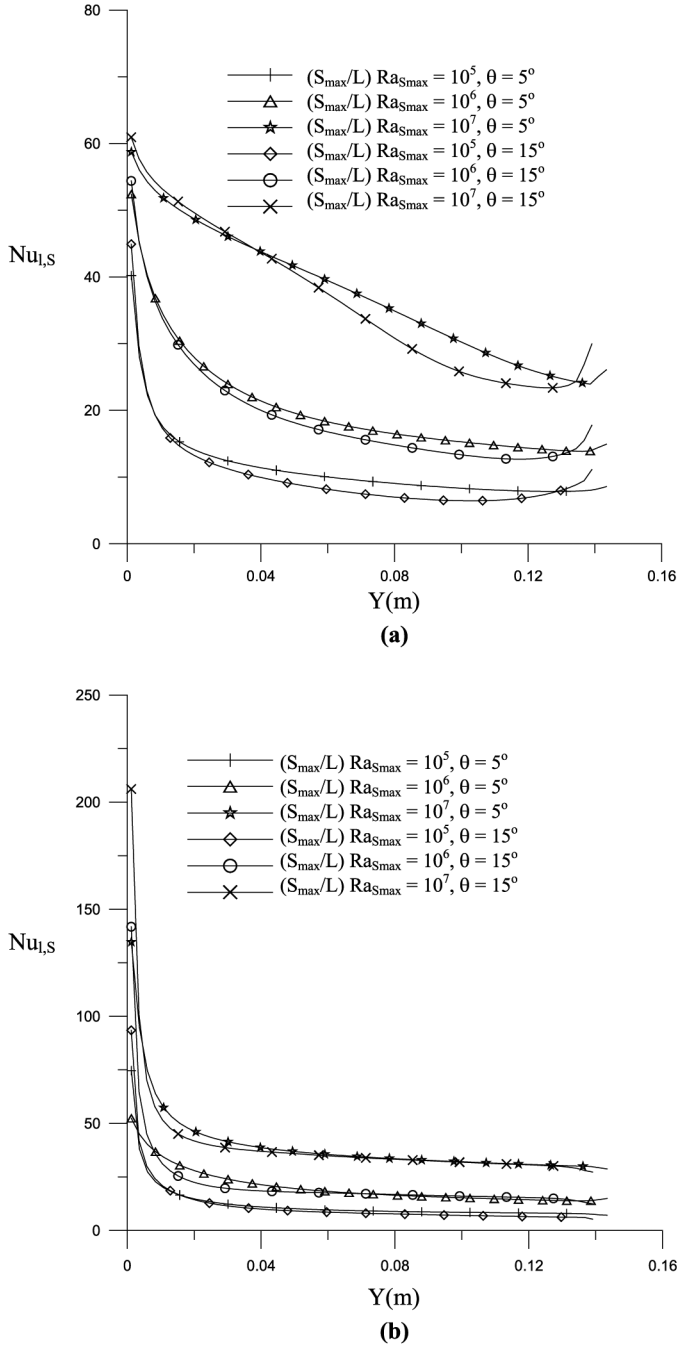

Figure 11.
Local Nusselt number for $Pr = 5.0$ and $L = 0.1452$ m
(a) convergent channel ($\theta = 5°$, $S_{max} = 0.03805$ m; $\theta = 15°$, $S_{max} = 0.0879$ m)
(b) divergent channel ($\theta = 5°$, $S_{max} = 0.03805$ m; $\theta = 15°$, $S_{max} = 0.0879$ m)

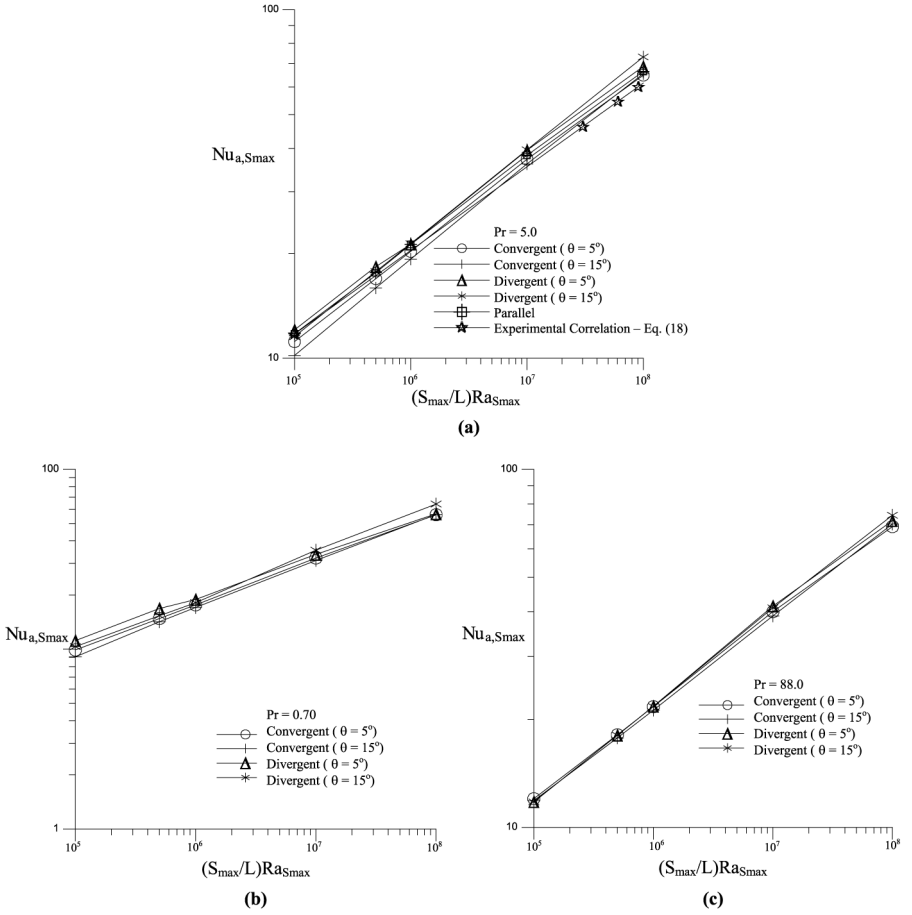

Figure 12.
Average Nusselt number (a) $Pr = 5.0$; (b) $Pr = 0.70$; (c) $Pr = 88$

Conclusions

This work presented solutions to natural convection in open parallel, convergent, and divergent channels using a fully elliptic procedure without extending the domains outside the channel for the application of boundary condition at the inlet and outlet of channel. The equations were solved by the finite-volume method using generalized coordinates and co-located arrangement. Results were shown for Prandtl number ranging from 0.7 to 88. For $Pr = 5$, a reasonable agreement with the experimental results available to the configurations studied was noticed. For convergent channels, a recirculation region in the outlet channel, which was not mentioned in the experimental data available in the literature, was observed. Although we believe that behavior to be completely possible, some additional effort is required to shed more light on this phenomenon. In any case, this recirculation does not alter the average Nusselt number. Finally, a new correlation that tries to put together all the results for the analyzed Prandtl numbers and configurations was proposed. A maximum deviation between the proposed correlation and simulated results was smaller than 19 percent.

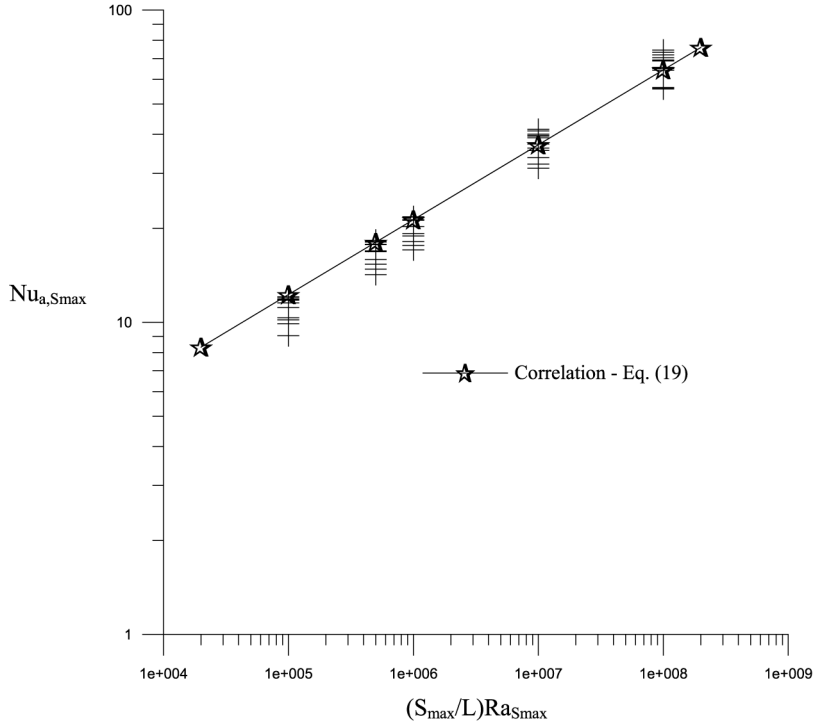

Figure 13.
Average Nusselt number for parallel, convergent, and divergent vertical channels ($\theta = 5°$ and $\theta = 15°$) and Prandtl numbers: 0.70, 5.0, and 88

References

Aihara, T. (1973), "Effects of inlet boundary condition on numerical solutions of free convection between vertical parallel plates", *Rep. Inst. High Speed Mech.*, Vol. 28, pp. 1-27.

Aung, W. and Worku, G. (1986), "Developing flow and flow reversal in vertical channel with asymmetric wall temperatures", *J. Heat Transfer*, Vol. 108, pp. 299-304.

Aung, W., Fletcher, L.S. and Sernas, V. (1972), "Developing laminar free convection between vertical flat plates with asymmetric heating", *Int. J. Heat Mass Transfer*, Vol. 15, pp. 2293-308.

Bejan, A. (1995), *Convection Heat Transfer*, 2nd ed., Wiley, New York, NY, p. 179.

Bodoia, J.R. and Osterle, J.F. (1962), "The development of free convection between vertical plates", *J. Heat Transfer*, Vol. 84, pp. 40-4.

Campo, A., Manca, O. and Morrone, B. (1999), "Numerical analysis of partially heated vertical parallel plates in natural convecting cooling", *Numerical Heat Transfer, Part A*, Vol. 36, pp. 129-51.

Da Silva, A.K., Bejan, A. and Lorente, S. (2004), "Maximal heat transfer density in vertical morphing channels with natural convection", *Numerical Heat Transfer, Part A*, Vol. 45, pp. 135-52.

Incropera, F.P. and DeWitt, D.P. (1990), *Introduction to Heat Transfer*, 2nd ed., Wiley, New York, NY, pp. 504-5.

Kaiser, A.S., Zamora, B. and Videma, A. (2004), "Correlation for Nusselt number in natural convection in vertical convergent channels at uniform wall temperature by a numerical investigation", *Int. J. Heat Fluid Flow*, Vol. 25, pp. 671-82.

Kettleborough, C.F. (1972), "Transient laminar free convection between heated vertical plates including entrance effects", *Int. J. Heat Mass Transfer*, Vol. 15, pp. 883-96.

Kihm, K.D., Kim, J.H. and Fletcher, L.S. (1993), "Investigation of natural convection heat transfer in converging channel flows using a Specklegram technique", *J. Heat Transfer*, Vol. 115, pp. 140-8.

Maliska, C.R. (1995), *Computational Fluid Mechanics and Heat Transfer*, LTC, Rio de Janeiro, pp. 135-137, 145-146, 185-186, (in Portuguese).

Maliska, C.R. and Marcondes, F. (1993), "Elliptic calculations of natural convection flows in arbitrary channels", *Proc. 8th Int. Conf. on Laminar and Turbulent Flow, Swansea, UK*, pp. 388-99.

Marcondes, F. and Maliska, C.R. (1999), "Treatment of the inlet boundary conditions in natural-convection flows in open-ended channels", *Numerical Heat Transfer, Part B*, Vol. 35, pp. 317-45.

Morrone, B. (2001), "Natural convection between parallel plates with conjugate conductive effects", *Numerical Heat Transfer, Part A*, Vol. 40, pp. 873-86.

Nakamura, H., Asako, Y. and Naitou, T. (1982), "Heat transfer by free convection between two parallel flat plates", *Numerical Heat Transfer*, Vol. 5, pp. 95-106.

Naylor, D., Florian, J.M. and Tarasuk, J.D. (1991), "A numerical study of developing free convection between isothermal vertical plates", *J. Heat Transfer*, Vol. 113, pp. 620-6.

Nieckele, A.O. and Azevedo, L.F.A. (1987), "Reverse flow in one sided heated vertical channels in natural convection", paper presented at ASME Winter Annual Meeting, Boston, pp. 71-7.

Peters, S., Marcondes, F. and Prata, A.T. (1993), "Numerical solution for natural convection between vertical and inclined asymmetrically heated parallel plates", *J. Brazilian Society Mechanical Sciences*, Vol. 15, pp. 368-75.

Raithby, G.D. and Torrance, K.E. (1974), "Upstream-weighted differencing schemes and their application to elliptic problems involving fluid flow", *Comp. Fluids*, Vol. 2, pp. 191-206.

Saad, Y. and Schultz, M.H. (1986), "GMRES: a generalized minimal residual algorithm for solving nonsymmetric linear systems", *SIAM J. Sci. Stat. Compt.*, Vol. 7, pp. 857-69.

Said, S.A.M. (1996), "Investigation of natural convection in convergent vertical channels", *Int. J. Energy Research*, Vol. 20, pp. 559-67.

Santos, L.A., Maliska, C.R. and Marchi, C.H. (1995), "The prime method for all speed flows using non-staggered grids", XIII Brazilian Congress of Mechanical Engineering, in CD-ROM, Belo Horizonte, Minas Gerais.

Shalash, J.S., Tarasuk, J.D. and Naylor, D. (1997), "Experimental and numerical studies of natural convection heat transfer in vertical converging channel flows", *Proc. Fourth Experimental Heat Transfer, Fluid Mechanics and Thermodynamics, Brussels, Belgium*, pp. 2167-74.

Sparrow, E.M. and Ruiz, R. (1988), "Experiments on natural convection in divergent vertical channels and correlation of divergent, convergent, and parallel-channel Nusselt numbers", *Int. J. Heat Transfer*, Vol. 31, pp. 2197-205.

Sparrow, E.M., Chrysler, G.M. and Azevedo, L.F. (1984), "Observed flow reversals and measured-predicted Nusselt numbers for natural convection in a one-sided heated vertical channel", *J. Heat Transfer*, Vol. 106, pp. 325-32.

Sparrow, E.M., Ruiz, R. and Azevedo, L.F.A. (1988), "Experimental and numerical investigation of natural convection in convergent vertical channels", *Int. J. Heat Mass Transfer*, Vol. 31, pp. 907-15.

Corresponding author
Francisco Marcondes can be contacted at: marconde@dem.ufc.br